Applied Catalysis B: Environmental 179 (2015) 29–36

Contents lists available at ScienceDirect

Applied Catalysis B: Environmental

journal homepage: www.elsevier.com/locate/apcatb

Enormous enhancement in photocatalytic performance of Ag_3PO_4/HAp composite: A Z-scheme mechanism insight

Yuanyuan Chai, Jing Ding, Li Wang, Qianqian Liu, Jia Ren, Wei-Lin Dai *

Department of Chemistry & Shanghai Key Laboratory of Molecular Catalysis and Innovative Materials, Fudan University, Shanghai 200433, PR China

ARTICLE INFO

Article history:
Received 9 March 2015
Received in revised form 30 April 2015
Accepted 3 May 2015
Available online 5 May 2015

Keywords:
Ag_3PO_4
HAp
Photocatalyst
Composite
Z-scheme mechanism

ABSTRACT

For the first time, the Ag_3PO_4/HAp composite catalysts were synthesized through a facile in-situ ion exchange method and carefully studied by various techniques including XRD, BET, SEM & TEM, DRS, ICP, XPS, ESR, and photocurrent measurements. It was found that the well dispersed small Ag_3PO_4 particles were loaded on the HAp support, and the surface area was slightly increased after the ion exchange process. Importantly, the coupling of the Ag_3PO_4 and HAp significantly enhanced the separation efficiency of the photogenerated electron–hole pairs and then promoted the activity for the photodegradation of RhB or 4-CP under visible light irradiation. What is more, the effect of calcination temperature of the HAp support on the catalytic performance was also discussed. It is interesting to find that the apparent rate constant of Ag_3PO_4/HAp-773 composite photocatalyst was 0.21 min^{-1}, which was 10 times higher than that of pristine Ag_3PO_4. The radical trapping experiments revealed that the introduction of HAp transformed the photocatalytic mechanism, which was obviously different from that of pure Ag_3PO_4. The enormous enhancement in catalytic performance may be attributed to the vacancy of HAp that resulted from the alternation in electronic state of surface PO_4 group under irradiation. Ultimately, a possible Z-scheme mechanism for the efficient Ag_3PO_4/HAp composite was proposed.

1. Introduction

In recent years, semiconductor photocatalysis has been viewed as an efficient technology for converting photon energy into chemical energy and for water treatment, in which one can use the sunlight as the sole energy source. This process can offer the possibility of accomplishing energy cycles without any pollution to the environment [1,2]. Unfortunately, the widely used photocatalyst, P25, is only active under UV-light irradiation accounting for about 3% of the solar spectrum [3]. Therefore, it is urgently necessary to synthesize more efficient visible light driven photocatalysis materials.

Interestingly, silver orthophosphate (Ag_3PO_4), a less common silver salt, demonstrates an extremely high quantum yield of about 80% at wavelengths less than 480 nm for O_2 evolution and degradation of organic contaminants [4–9]. The photocatalytic performance of Ag_3PO_4 is significantly higher than that of currently known visible light photocatalyst, such as N-TiO_2 and $BiVO_4$ [9,10]. However, it should be noted that there are still some limitations in the Ag_3PO_4 photocatalytic system. First of all, as the electrode potential of Ag_3PO_4/Ag (around 0.45 V vs. NHE) in aqueous solution is more positive than that of H^+/H_2 (0 V vs. NHE) [11], Ag_3PO_4 can easily be reduced to Ag^0 during the photocatalytic reactions. In addition, the potential of the conduction band (CB) is more positive than the reduction potential of O_2 ($O_2 + e^- \rightarrow {}^{\bullet}O_2^-$ −0.33 V vs. NHE) [12]. As a result, the generated electrons cannot be consumed by combining with O_2, which is very important for the photodegradation of various pollutants. Therefore, the electrons cannot efficiently react with substrate molecule, hindering its performance in photocatalytic process and decreasing the stability. Thus, much attention has been employed to develop a simple and effective technology to improve efficiency of photoinduced electrons for Ag_3PO_4 system. Constructing a hybrid or heterojunction between Ag_3PO_4 and another semiconductor with proper band structure such as Ag_3PO_4/TiO_2 [13], Ag_3PO_4/g-C_3N_4 [10,14], Ag_3PO_4/SnO_2 [15], Ag_3PO_4/Ag/SiC [16], Ag_3PO_4-Graphene [17], and P25/Ag_3PO_4/graphene oxide [18] can enhance the photocatalytic activity and stability of Ag_3PO_4 in the photocatalytic degradation of organic pollutants and bacteria. Moreover, the particles size of Ag_3PO_4 has obvious effect on the efficiency of photodegradation [19]. Ag_3PO_4 is easily precipitated in the solution, and the particle size remains relatively large (0.5–2 μm), which hinders their practical application. Recent reports indicated that Ag_3PO_4 immobilized in bentonite could improve its photocatalytic activity and stability

* Corresponding author. Tel.: +86 5566 4678; fax: +86 5566 5572.
E-mail address: wldai@fudan.edu.cn (W.-L. Dai).

http://dx.doi.org/10.1016/j.apcatb.2015.05.006
0926-3373/

[20]. Therefore, more and more studies have focused on the appropriate supporter for Ag_3PO_4 catalyst to enhance the stability and performance of the as-prepared composite photocatalysts.

Hydroxyapatite, $Ca_{10}(PO_4)_6(OH)_2$, abbreviated as HAp, is not only a main component of hard tissues, such as bones and teeth, but a material is applied for bioceramics, adsorbents, and catalysts [21]. Concerning the electronic structure, HAp is a naturally sourced, wide band-gap semiconductor [22,23]. Unlike its applicability in regenerative medicine, its potential biomedical usage in the form of a photocatalyst has not been so extensively studied. As a photocatalyst, HAp exhibited its own photocatalytic activity in the decomposition of several toxic organic compounds, such as propane and propene [24], and dimethyl sulfide [25]. It was suggested that the photocatalytic activity of HAp is caused by the generation of active superoxide anion radicals due to alteration in the electronic state of surface PO_4^{3-} group under UV irradiation [26–28]. Furthermore, the presence of a PO_4-sublattice together with Ca-channels makes them highly acceptable for a variety of ion-exchanges. These structural changes are suitable for inducing significant variations in the electronic structure, which provides a useful possibility for the modulation of the band gap of HAp, so affecting their optical properties [29]. It has been reported that the doping of HAp with different ions (Cr^{3+}, Zn^{2+}, and Fe^{3+}) provides a broadening of the adsorption band of HAp from the UV to the vis region [30]. The latter was considered to be an interesting tool for applications in sunscreen production. Therefore, HAp can be served as a catalyst support thanks to its high specific surface areas [31] and versatile ion-exchange property [32]. Thus, there are several reports about the significant improvement in photocatalytic performance for the combination of TiO_2 and HAp, which was assigned to the synergetic effect of high photocatalytic activity of TiO_2 and the high adsorption ability of HAp [33–35]. Additionally, silver carrying nano-hydroxyapatite was firstly synthesized by simple wet impregnation method for the application of antibacterial [36]. Hong et al. reported that HAp may act as an adsorbent which favors the mass transfer for heterogeneous photocatalysis reaction in the Ag_3PO_4/HAp system [37]. However, there is no intensive discussion about the improvement for the doping of HAp with Ag-ions. And an issue regarding the transfer route of the photoexcited charges in the system still persists.

In the present work, a kind of highly efficient Ag_3PO_4/HAp catalyst was synthesized through a facile one-step in-situ ion exchange method with HAp microsphere as the support. In order to interpret how the photocatalysis of Ag_3PO_4 is affected by the support, the photodegradation of Rhodamine B (RhB) and 4-cholorphenol (4-CP) under visible light was chosen as probe reaction. The photocatalytic activity of Ag_3PO_4/HAp was enhanced about 10 times as compared to the pristine Ag_3PO_4. To the best of our knowledge, this is the first time where the as-prepared catalyst is systematically studied to investigate the relationship between the structure–function and the activity behavior of pollutants degradation. After thorough analysis of the trapping experiment, ESR technique and the photocurrent measurement, the Z-scheme mechanism of the Ag_3PO_4/HAp composite was proposed.

2. Experimental

2.1. Catalyst preparation

All the reagents are purchased from Sinopharm Chemical Reagent Co., Ltd., without further purification, unless otherwise specified.

Synthesis of pure HAp: microsphere HAp is synthesized via a facile hydrothermal method. Typically, calcium nitrate ($Ca(NO_3)_2{\cdot}4H_2O$, 9.41 g), di-ammonium hydrogen phosphate ($(NH_4)_2HPO_4$, 3.16 g), and urea ($CO(NH_2)_2$, 3.60 g) were dissolved in 120 mL of deionized water with vigorous stirring. Meanwhile, a certain amount of nitric acid was added into the above solution to adjust the pH value below 3.0. After that, the as-obtained suspension was kept on stirring for 15 min, and then the pH value of the suspension reached 3.0 with the addition of aqueous ammonia. After that, the resulting suspension was poured into a Teflon-lined stainless steel autoclave and heated up to 423 K for 24 h. Finally, the obtained precipitates were washed with deionized water for three times. The solid was dried at 373 K overnight, and then calcinated from 473 to 973 K at a ramping rate of 2 K min^{-1}.

Synthesis of Ag_3PO_4/HAp composite photocatalyst: the deposition of Ag_3PO_4 nanoparticles onto the HAp was carried out by an in-situ ion exchange method. In short, 0.30 g HAp was firstly added to 30 mL H_2O and the suspension was stirred intensively for 30 min. Meanwhile, 0.04 g $AgNO_3$ powder was dissolved in 30 mL of distilled water and stirred for 10 min. Then, a 10.0 wt% ammonia solution was added into the above solution to obtain the silver-ammine complex. After that, the silver-ammine solution was mixed with the suspension of HAp and stirred for additional 5 h. Finally, the supernatant fluid was removed from the precipitate by centrifugation, and the remaining precipitates were dried overnight in a vacuum oven at 333 K.

The HAp support at different calcination temperatures was further studied to confirm the structural evolution and the distinct catalytic sites on the catalysts. These catalysts were labeled as Ag_3PO_4/HAp-*y*, where *y* denotes the calcination temperatures (*K*). For comparison, pure Ag_3PO_4 particles were also prepared by adding $AgNO_3$ solution to some amount of Na_3PO_4 solution dropwisely, and then the as-obtained Ag_3PO_4 was centrifuged, collected, and dried under the same condition.

2.2. Catalyst characterization

The wide-angle XRD patterns were collected on a Bruker D8 Advance X-ray diffractometer using nickel-filtered Cu *Kα* radiation ($\lambda = 0.15406$ nm) with a scanning angle (2θ) range of 20–90°, a scanning speed of 2° min^{-1}, and a voltage and current of 40 kV and 40 mA, respectively. The full width at half maximum (FWHM) of Ag_3PO_4 (2 1 0) reflection was measured for calculating crystallite sizes using the Scherrer equation.

Specific surface areas of the samples were measured by nitrogen adsorption–desorption method at 77 K (Micromeritics Tristar ASAP 3000) using Brunauer–Emmett–Teller (BET) method.

Scanning electron micrographs (SEM) were obtained using a PHILIPS XL 30 microscope operating at accelerating voltage of 20 kV. TEM micrographs were obtained on a JOEL JEM 2010 transmission electron microscope. Samples for electron microscopy observation were prepared by grinding and subsequent dispersing the powder in ethanol and applying a drop of very dilute suspension on carbon coated grids.

The optical properties of the samples were analyzed by UV–vis diffuse reflectance spectroscopy (DRS) using a UV–vis spectrophotometer (Cary-500, Varian Co.), in which $BaSO_4$ was used as the internal reflectance standard.

The Ag_3PO_4 loadings were determined by the inductively coupled plasma (ICP) method using a Thermo Electron IRIS Intrepid II XSP spectrometer (PerkinElmer, 8000).

X-ray photoelectron spectroscopy (XPS) experiments were carried out with a RBD 147 upgraded PerkinElmer PHI 5000C ESCA system equipped with a hemispherical electron energy analyzer. The Mg *Kα* ($h\nu = 1253.6$ eV) anode is operated at 14 kV and 20 mA. The spectra were recorded in the constant pass energy mode with a value of 46.95 eV, and all binding energies were calibrated using the carbonaceous C 1s line at 284.6 eV as reference. The experimental errors were within ±0.2 eV.

A Bruker model A300 spectrometer equipped with a Xe lamp (with 420 nm filter) was used for measurements of the electron spin resonance (ESR) signals of radicals spin trapped by DMPO.

Electrochemical measurements were performed by using a CHI 660B electrochemical work station with a standard three-electrode cell at room temperature. The as-prepared sample, an Ag/AgCl (saturated KCl), and a Pt wire are used as the working electrode, the reference electrode, and the counter electrode, respectively. Na_2SO_4 (0.5 M) was used as the electrolyte solution. A suspension of 200 mg of the powder in 1 mL of absolute ethanol was used for casting onto the ITO glass substrate. The coated glass was then heated at 373 K in air for 1 h to improve adhesion.

2.3. Catalytic activity test

Photo-catalysts for RhB and 4-CP degradation were tested under visible light irradiation. The photo-reactor was equipped with a cooling jacket to maintain the temperature at 293 K and a 300 W Xe arc lamp (CeauLight, CEL-HXF300) equipped with an ultraviolet cutoff filter ($\lambda \geq 420$ nm). The photo-catalysts were maintained in suspension with a magnetic stirrer. The entire setup was placed in a tightly closed compartment to avoid interferences from ambient light. The substrate solution (100 mL, 10 mg/L) containing 0.150 g of Ag_3PO_4/HAp-*x* or 0.050 g of pure Ag_3PO_4 was placed in the photo-reactor. The trapping experiments of radicals and holes were performed according to the methods from Ref. [38]. For instance, 0.01 mL of isopropanol (IPA) used as hydroxyl radical (•OH) scavenger, were added to the above mentioned reaction system. In addition, 0.01 g of benzoquinone (BQ) was added as superoxide radical ($^{\bullet}O_2^-$) scavenger and 0.01 g of EDTA as hole (h^+) scavenger.

In all experiments, the suspensions were stirred in the dark for 30 min prior to irradiation to achieve the adsorption/desorption equilibrium. After turning on the lamp, 5 mL suspensions were sampled at known time intervals and centrifuged (Shanghai Anting Scientific Instrument Factory, China) to remove the photo-catalyst. The degradation of organic dyes was monitored by UV–vis spectroscopy (721, Shanghai Jing-ying). The degradation efficiency can be calculated using the following equation:

$$\text{Degradationefficiency} = \frac{(C_0 - C)}{C} \times 100\%$$

where C_0 is the initial concentration of RhB before illumination (mg/L) and C is the concentration of RhB after a certain illumination time period t (min).

3. Results and discussion

3.1. The formation mechanism of Ag_3PO_4/HAp

HAp microsphere was obtained by simple hydrothermal method without template-directed regents. Ag_3PO_4/HAp was synthesized by a facile one-step in-situ ion exchange method using a clear silver ammine solution as Ag sources. The formation process of Ag_3PO_4 onto HAp is illustrated in Scheme 1. The presence of a PO_4-sublattice together with Ca-channels makes them highly acceptable for a variety of ion-exchanges [39]. Additionally, the pH of the suspension for HAp powder is higher than 7.0. Therefore, positively charged silver ammine ions could be adsorbed onto the surface of HAp, and then tend to react with the PO_4^{3-} in the crystal of HAp because of the lower solubility product of Ag_3PO_4 ($K_{sp} = 1.4 \times 10^{-16}$).

3.2. Characterization of the Ag_3PO_4/HAp composite

The X-ray diffraction patterns (XRD) of the as-prepared HAp, Ag_3PO_4, and Ag_3PO_4/HAp-773 are shown in Fig. 1. The indexed

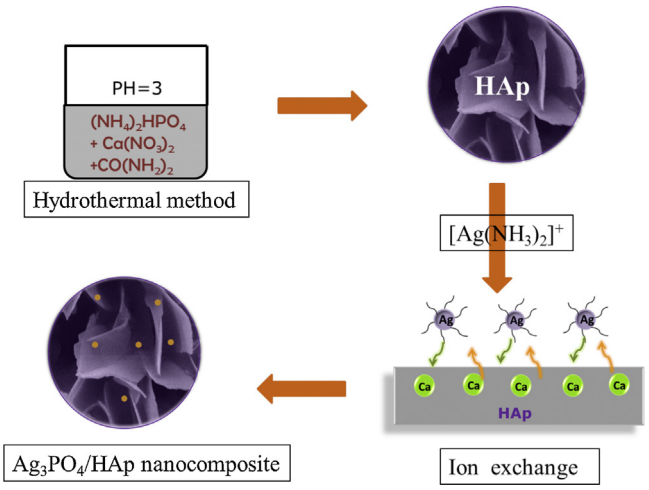

Scheme 1. The schematic diagram of the formation process of Ag_3PO_4/HAp by a facile one-step in-situ ion-exchange method.

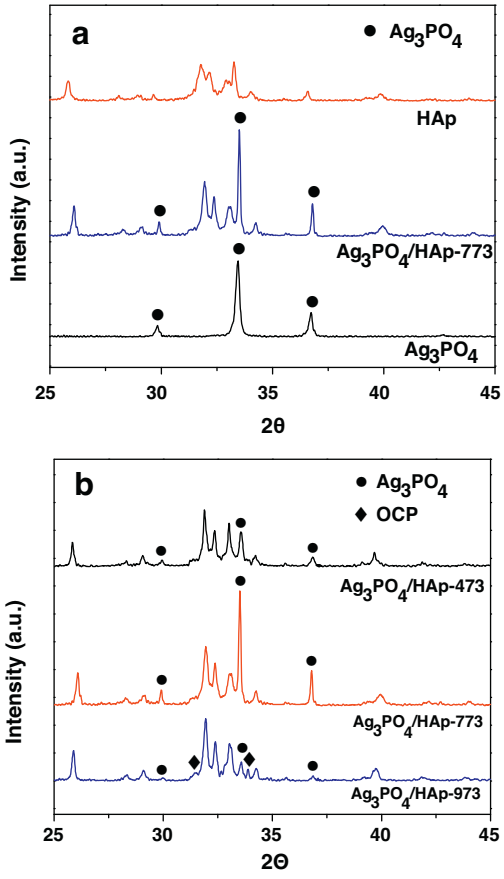

Fig. 1. XRD patterns of HAp, Ag_3PO_4 and Ag_3PO_4/HAp-773 (a), and Ag_3PO_4/HAp-*y* (b).

diffraction peaks can be ascribed to Ag_3PO_4 and HAp, indicating that the Ag_3PO_4 did not affect the crystal structure of HAp. Uniform 3D structured HAp flowers with smooth surface nanosheet-constructed network are presented in Fig. 2(a and b). For Ag_3PO_4/HAp-773 composite photocatalyst, the surface of HAp nanosheet becomes slightly rough due to the formation of Ag_3PO_4 (Fig. 2c). However, there is no appreciable change in their overall morphologies during ion-exchange process. The corresponding EDX pattern displays the presence of Ag, Ca, O, and P elements

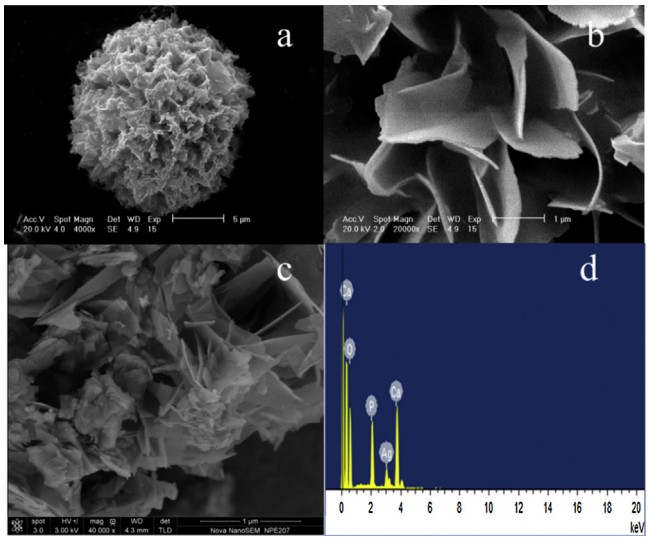

Fig. 2. SEM images of pure HAp (a–b), and Ag_3PO_4/HAp-773 composite (c); the corresponding EDS pattern for Ag_3PO_4/HAp-773 composite (d).

(Fig. 2d). The TEM image is shown in Fig. 3(a and b), and the Ag_3PO_4 particles with size of 10–15 nm were distributed homogeneously on the supports. In addition, the HRTEM image declares the lattice fringes which fit well with the HAp (1 0 1) and HAp (1 0 0) planes, confirming the existence of the crystalline HAp structure. The lattice fringe of 0.239 and 0.264 nm, respectively, corresponding to the Ag_3PO_4 (2 1 1) and Ag_3PO_4 (2 1 0) planes reveals the successful synthesis of Ag_3PO_4/HAp composite and the well connection between Ag_3PO_4 with HAp supporter, which may promote the electron transfer between them (Fig. 3c). The EDX mapping can further demonstrate this observation. Fig. 3(d–f) exhibits the Ca, P, and O elements that belong to the HAp support. Moreover, it is clearly found that some relative large and bright particles are presented in Fig. 3g, which was believed to originate from the formation of Ag_3PO_4 nanoparticles during the ions-exchange process. The results distinctly indicate that the Ag_3PO_4 nanoparticles were

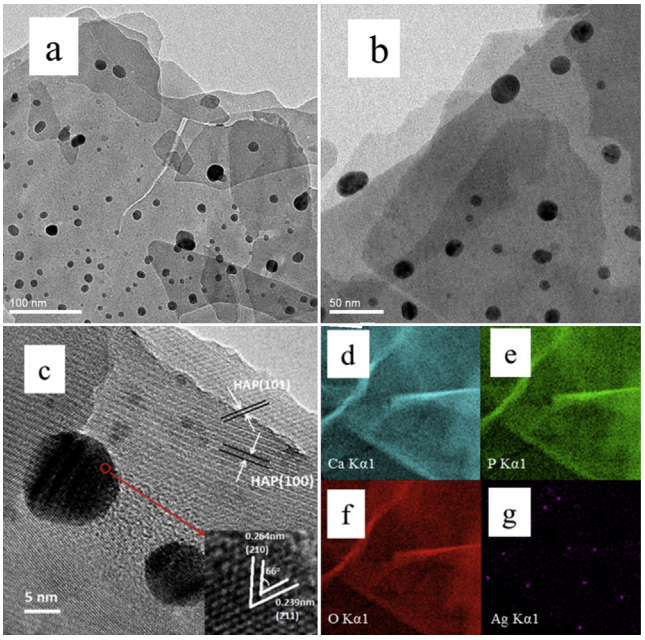

Fig. 3. TEM images (a–b), HRTEM images (c), and Ca, P, O. and Ag element mapping images (d–g) of Ag_3PO_4/HAp-773.

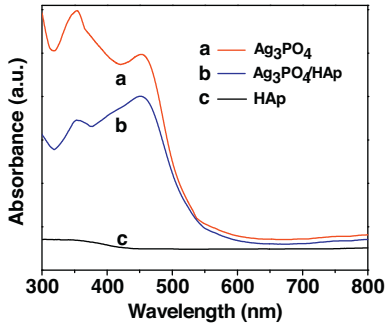

Fig. 4. UV–vis diffuse reflectance spectra of HAp, Ag_3PO_4, and Ag_3PO_4/HAp.

well dispersed on the surface of HAp, revealing that HAp can be served as a proper carrier. The results of the XPS analysis also confirm the coexistence of Ag_3PO_4 and HAp (Fig. S1). Additionally, the UV–vis DRS of HAp, Ag_3PO_4, and Ag_3PO_4/HAp-773 composite are presented in Fig. 4. It can be clearly seen that the Ag_3PO_4/HAp can absorb solar energy with a wavelength shorter than ~530 nm, which corresponds well with the finding reported by Yi et al. [4]. The UV–vis DRS analysis implies that the Ag_3PO_4/HAp-773 composite is a potential photo-catalyst for visible light degradation.

3.3. *Photocatalytic activities of Ag_3PO_4, HAp and Ag_3PO_4/HAp-y*

The photocatalytic performance of the HAp, Ag_3PO_4, and Ag_3PO_4/HAp-773 was first evaluated by the degradation of model molecule RhB under visible light irradiation ($\lambda > 420$ nm). Only 2% RhB was degraded under visible light irradiation in the absence of photocatalyst (see Fig. S2). As shown in Fig. 5a, it could be observed that 97% of the RhB was degraded within 20 min of irradiation over the Ag_3PO_4/HAp-773 composite photocatalyst. Obviously, the photocatalytic activities of the pure HAp and Ag_3PO_4 were extremely lower than that of the composite photocatalyst. The Ag_3PO_4 decolorized 60% of the RhB solution after 40 min of irradiation, while the HAp exhibited even negligible activity.

The kinetics of the photocatalytic degradation can be described using the pseudo-first-order reaction. The apparent rate constants calculated based on regression curves of $\ln(C/C_0)$ vs. irradiation time was 0.0002 min^{-1} for HAp (Fig. 5b). As listed in Table 1, it clearly demonstrated that the apparent rate constant of Ag_3PO_4/HAp-773 composite photocatalyst, about 0.21 min^{-1}, is 10 times higher than that of pure Ag_3PO_4. Moreover, the Ag_3PO_4/HAp-com, using the commercial HAp as the support, was also investigated. Although the rate of degradation is higher than that of pristine Ag_3PO_4, it is still lower than that of Ag_3PO_4/HAp-773 composite. The enhanced photcatalytic activity may be resulted from the microsphere morphology of the Ag_3PO_4/HAp-773, which would greatly accelerate the transfer of dye molecule in the reaction. In addition, Ag_3PO_4/HAp-773 composite exhibited excellent activity for 4-chlorophenol (4-CP), methyl orange (MO), and methylene blue (MB) degradation (Fig. 5c and Fig. S3). Therefore, the Ag_3PO_4/HAp-773 composite photocatalyst possesses dramatically

Table 1
Physicochemical parameters and the reaction rate of different catalysts.

Sample	BET (m^2/g)	k (min^{-1})	Ag_3PO_4 loading (wt%)[a]
HAp	21.0	0.0002	–
Ag_3PO_4	2.1	0.0211	–
Ag_3PO_4/HAp-473	25.0	0.0421	7.7
Ag_3PO_4/HAp-773	24.2	0.2071	11.0
Ag_3PO_4/HAp-973	17.5	0.0166	7.1
Ag_3PO_4/HAp-com	20.8	0.0601	8.0

[a] Weight percentage of Ag_3PO_4 measured by ICP.

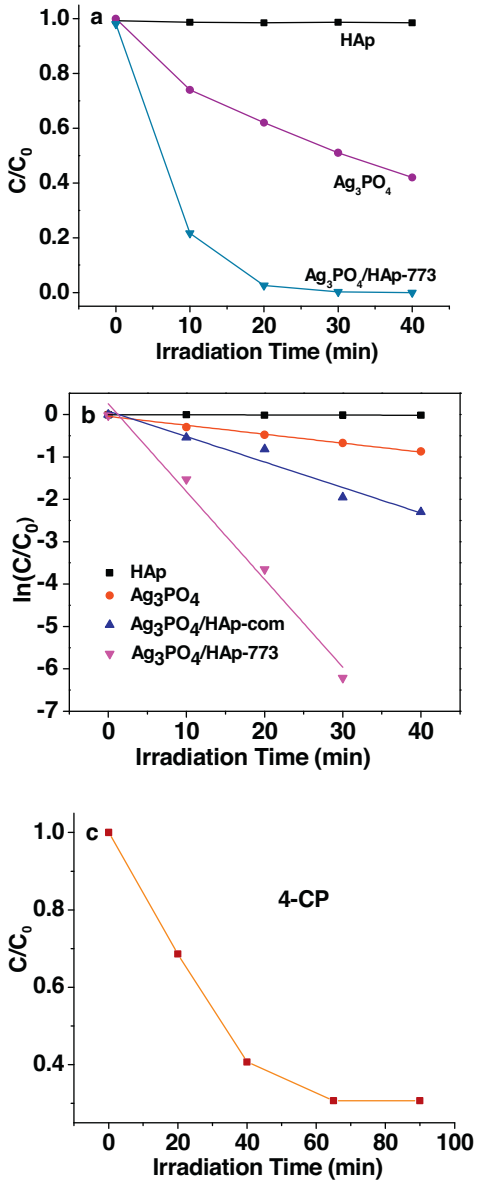

Fig. 5. Photoactivity and the apparent rate constants for the degradation of RhB over HAp, Ag_3PO_4, and Ag_3PO_4/HAp-773 (a–b); photodegradation of 4-CP over Ag_3PO_4/HAp-773 catalyst (c), under visible light irradiation.

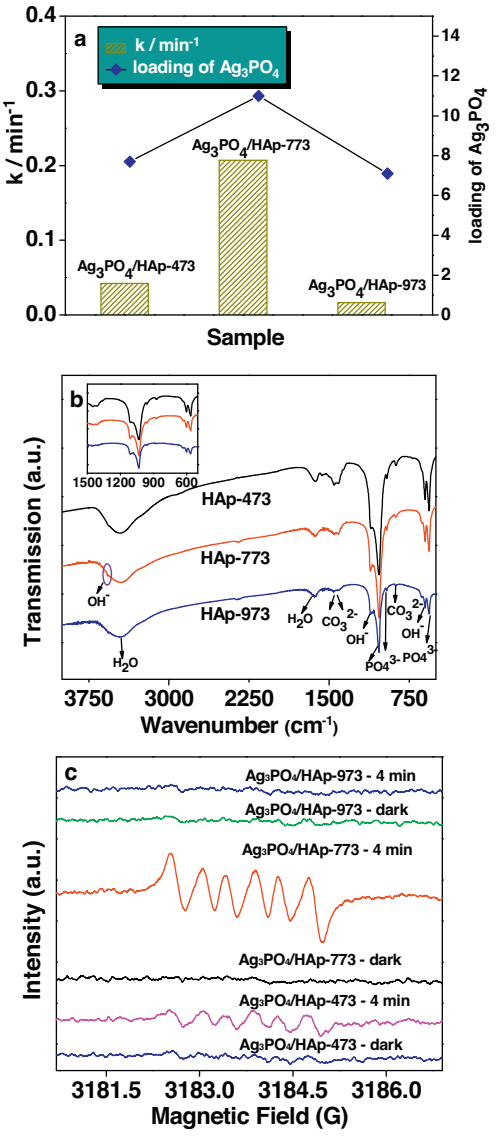

Fig. 6. Photoactivity for RhB and the loading of Ag_3PO_4 calculated from ICP over Ag_3PO_4/HAp-*y* (a); FT-IR spectra the prepared HAp with calcination at 473, 773, and 973 K (b); ESR signals Ag_3PO_4/HAp-*y* (c).

enhanced activity in the photocatalytic decomposition of various pollutants.

Interestingly, we found that the calcination temperature of HAp in the composite has great influence on the photoactivity. As given in Fig. 6a, the Ag_3PO_4/HAp-473 sample with calcination at 473 K exhibited a relatively low photocatalytic activity. With the calcination temperature increasing to 773 K, the photocatalytic activity significantly increased, while its catalytic performance decreased obviously at 973 K. It is obviously found that the reaction rate constant of Ag_3PO_4/HAp-773 was 4.9 and 13 times as high as those of Ag_3PO_4/HAp-473 and Ag_3PO_4/HAp-973 for the RhB degradation, respectively.

As well known, the surface area is a crucial factor for the heterogeneous catalysis. However, there is no visible difference in BET surface area among different catalysts (Table 1). Obviously, the enhancement of photocatalytic activities cannot be attributed to the BET surface area of the samples. To clarify the calcination temperature effects on the photocatalytic activity enhancement, we further studied the relationship of the intrinsic structure and the catalytic performance. Fig. 6b shows the FT-IR absorption spectra of the samples. The peaks at 471, 563, 602, 960, and 1030 cm^{-1} were assigned to the PO_4^{3-} [40]. The peaks at 3570, 1260, and 630 cm^{-1} were regarded as OH bands of hydroxyapatite. From the inset, it is found that the intensity of these hydroxyl groups for HAp with calcination at 773 K was distinctly stronger than that of others. Furthermore, according to the previous reports [38,41], the rough estimation of C_{OH} is about 1.7×10^{19}, 2.2×10^{19} and 1.0×10^{19} cm^{-3} for HAp calculated at 473, 773, and 973 K, respectively. In addition, the weak bimodal peaks at 1412, 1446, and 872 cm^{-1} are the characteristic bands for carbonate ion in the B-site [42]. B-site substitution indicates that $[CO_3 \cdot OH]^{3-}$ tetrahedron replaces $[PO_4]^{3-}$, when OH groups exist simultaneously at two sites: $[CO_3 \cdot OH]^{3-}$ tetrahedron site and OH channel site [43], and then consequentially decreases the content of PO_4^{3-} and induces crystal lattice aberrance. Therefore, the HAp with calcination at 773 K had enough OH on the channel site and PO_4^{3-}, which facilitate the immobilized Ag species on the HAp support. The above speculation was further confirmed by the analysis of XRD and ICP. Fig. 1b presents the XRD patterns of the Ag_3PO_4/HAp-*y*

composite. The intensity of the Ag_3PO_4 was the strongest, revealing that the silver species could efficiently react with the PO_4^{3-} in HAp to form Ag_3PO_4/HAp-773 composite. As we can see, with the increase of calcination temperature to 973 K, there appears a small portion of octacalcium phosphate ($Ca_8(HPO_4)_2$-$(PO4)_4{\cdot}5H_2O$, OCP) phase, which may be adverse to the formation of Ag_3PO_4. And the practical loading of Ag_3PO_4 that calculated from the ICP method was higher for Ag_3PO_4/HAp-773 than those of the others, which is in accordance with the XRD results, as proven in Table 1. Therefore, the difference in photoactivity is mainly ascribed to the surface structure of HAp, which played an important role in the ion-exchange process.

3.4. The mechanism of the enhanced photocatalytic activity

It is generally accepted that the high surface area, good light absorption capability, and high separation efficiency of electron–hole pairs are beneficial for the performance of a photocatalyst. As listed in Table 1, the BET area of Ag_3PO_4/HAp-773 composite was slightly higher than that of Ag_3PO_4. In addition, the smaller particle size and the well dispersion of the Ag_3PO_4 also accelerated the photodegradation, however, these factors could not explain its significantly high photoactivity. Therefore, the effect of the Ag_3PO_4/HAp-773 (b) composite on the separation efficiency of electron–hole pairs was investigated by photoelectric current experiments, as demonstrated in Fig. 7a. Although all these samples showed a quick response to the light either on or off, the generated transient photocurrent is totally different. There is almost no photocurrent on pure HAp (c). However, it can be found that the photocurrent over Ag_3PO_4/HAp-773 was about two times higher than that of pure Ag_3PO_4 (a), which suggested more efficient separation of the photogenerated electron–hole pairs over Ag_3PO_4/HAp-773. Meanwhile, the order is in good agreement with the result of the photoactivity (Fig. 5a).

In order to reveal the dramatic activity enhancement and the internal mechanism of the as-prepared composite, the main oxidative species in the photocatalytic process were explored through the trapping experiments of radicals and holes. As presented in Fig. 7b, the photocatalytic activity of Ag_3PO_4/HAp-773 catalyst was almost invariable by the addition of a hydroxyl radical scavenger. On the other hand, the addition of EDTA and BQ made the rate of RhB degradation decrease from 0.21 to 0.0045 and 0.005 min^{-1}, indicating that $^{\bullet}O_2^-$ and h^+ bi-reactive species are the main oxidative centers in the Ag_3PO_4/HAp-773 system. By using the same method, the reactive species trapping experiments were also carried out for pure Ag_3PO_4. The results (Fig. 7c) certified that h^+ is the main oxidative species in pristine Ag_3PO_4 material, which is consistent with the previous literature [44]. Based on the above analysis, it can be concluded that the photooxidation process occurring on the surface of Ag_3PO_4/HAp-773 sample may involve the direct reaction of the pollutants with strong oxidizing superoxide radicals and holes. These results revealed that the photodegradation mechanism of Ag_3PO_4/HAp-773 catalyst has been changed, if compared with that of pure Ag_3PO_4.

ESR spectroscopy with a spin trapping method was employed to further investigate the involvement of $^{\bullet}O_2^-$ radical species in the photocatalytic process of Ag_3PO_4/HAp. As shown in Fig. 7d, the ESR spectra of DMPO-trapped $^{\bullet}O_2^-$ in methanol have been investigated. For all the samples, no ESR characteristic signals were detectable for the sample without light irradiation. Under visible light irradiation for 4 min, six characteristic peaks of the DMPO-$^{\bullet}O_2^-$ adducts were observed. It is clearly seen that the intensity of the peaks attributed to DMPO-$^{\bullet}O_2^-$ was 3 times higher than that for pure Ag_3PO_4. Therefore, the results also proved the presence of the more superoxide radicals in the photodegradation process, which strongly agrees with the results of the reactive species trapping

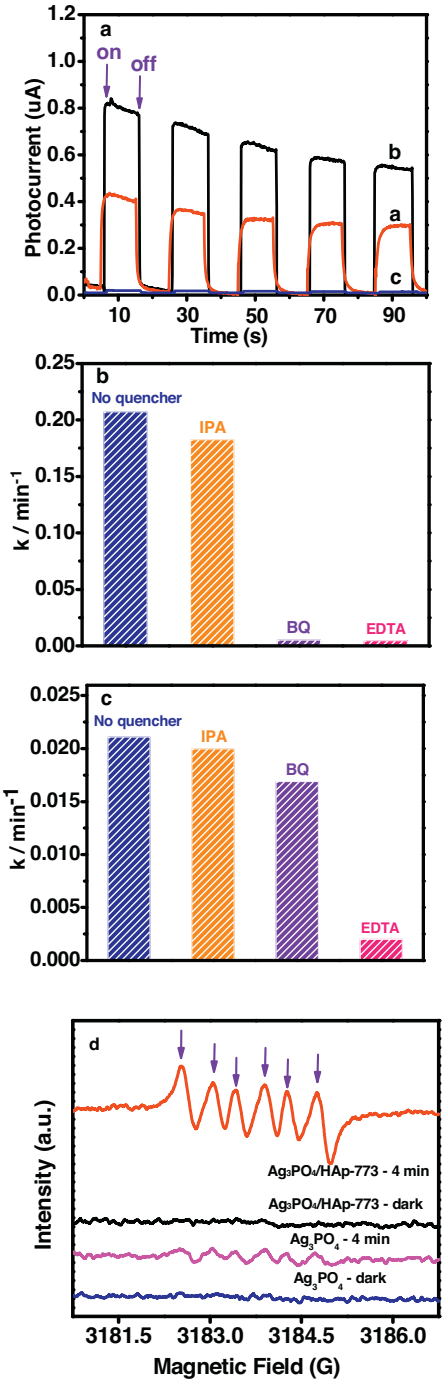

Fig. 7. Transient photocurrent responses of HAp, Ag_3PO_4, and Ag_3PO_4/HAp-773 (a); effects of various scavengers on the photocatalytic efficiency of Ag_3PO_4/HAp-773 (b), and pure Ag_3PO_4 (c); ESR signals of Ag_3PO_4 and Ag_3PO_4/HAp-773 (d).

experiments. In addition, a much stronger ESR signal was produced on the Ag_3PO_4/HAp-773 photocatalyst than on other samples, indicating more superoxide species were generated during the irradiation of Ag_3PO_4/HAp-773. This finding is well consistent with the order of the photoactivity (Fig. 6 (a and c)). This result may be related to the content of the Ag_3PO_4 and the surface structure of HAp, which was discussed in the context.

As we know, there are two pathways for the photodegradation of RhB. One is the cleavage of the all-conjugated structure, with the main absorption peak (~554 nm) shrinking, whereas the location does not shift. The other is de-ethylation at the nitrogen,

which features the blue-shift of the absorption peak to 498 nm [45]. The temporal UV–vis absorption spectral change during photodegradation of the RhB solution on Ag_3PO_4/HAp-773 catalyst is shown in Fig. 8a. It is clear that the intensity of the absorbance at 554 nm significantly declined during the decoloration process in the Ag_3PO_4/HAp-773 system, while there is no obvious shift. Therefore, the diminishment of the absorption band demonstrated the complete structural cleavage of RhB by the superoxide radical, which is in agreement with the previous reports [38,46].

Based on the above discussion, the coupling effect of Ag_3PO_4 and HAp was believed to play a more important role in the photocatalytic reaction. Compared with the pristine Ag_3PO_4 system, the bi-reactive species ($^{\bullet}O_2^-$ and h^+) and higher separation efficiency for the Ag_3PO_4/HAp-773, mainly improve the catalytic performance. Under visible light irradiation, the electrons in valance band of Ag_3PO_4 can be excited to the conduction band, leaving the holes in the valence band. Normally, due to the more negative potential of $O_2/^{\bullet}O_2^-$ (−0.33 eV vs. NHE), the photo-generated electrons tended to in situ reduce Ag^+ to metallic Ag rather than generated the superoxide radicals, as illustrated in Fig. 8b. Such a mechanism cannot declare the generation of the superoxide radical for the Ag_3PO_4/HAp-773 composite. Meanwhile, the formation of the oxygen vacancy for HAp under irradiation was useful in deducing the charge transmission route in the composite. Thus, a possible Z-scheme mechanism for the photocatalytic degradation of pollutant over Ag_3PO_4/HAp-773 composite was proposed.

As illustrated in Fig. 8b, the produced vacancy on HAp might act as a charge transmission bridge to form the Ag_3PO_4/HAp-773 Z-scheme system. As a result, the connection between Ag_3PO_4 and HAp made the electrons on the CB of Ag_3PO_4 transfer to HAp support due to electro-conductivity resulted from the alternation in electron state of surface PO_4 group under light irradiation. According to the literature reports, these changes may lead to the formation of vacancies on the surface of HAp [26]. Then

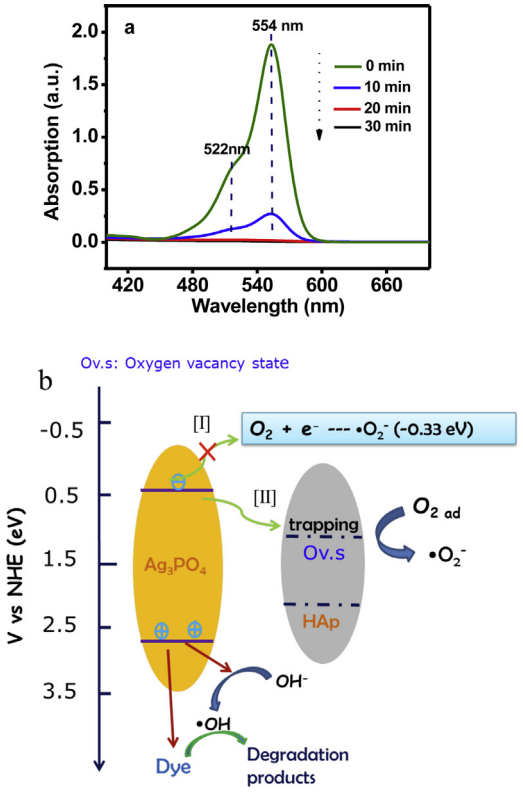

Fig. 8. UV–vis absorption spectra of reaction intermediates on Ag_3PO_4/HAp-773 (a); photocatalysis mechanism of the Ag_3PO_4/HAp composite (b).

the holes were capable of oxidizing pollutants directly, simultaneously, the accumulated electrons on the HAp were easily trapped by the adsorbed O_2 on the vacancies to form superoxide radical ($^{\bullet}O_2^-$), and then took part in the photooxidation. This type of charge transmission efficiency enhances the separation of electron–hole pairs and enables the electrons and the holes to remain on the vacancy of HAp and the VB of Ag_3PO_4, respectively. Hence, the electrons were captured by the absorbed oxygen on the vacancy of HAp only when the electron and hole in the Ag_3PO_4/HAp-773 migrated by the Z-scheme mechanism. In other words, the photoexcited electrons would accumulate on the vacancy of HAp that creates the superoxide radical and results in another dominant reactive species of h^+, which directly improve the photocatalytic performance. Although the photocatalytic reaction rate decreased in the first three cycling run, the Ag_3PO_4/HAp-773 exhibited much higher activity than that of the pure Ag_3PO_4 (Fig. S4). This decline might be ascribed to the instability of the vacancy in the HAp or the photo-reduction of a part of Ag^+ by the redundant electrons that generated from Ag_3PO_4. Furthermore, the mass percentage of Ag was about 3.0% in the used Ag_3PO_4/HAp-773 catalyst, implying that 20% Ag_3PO_4 was reduced during the reaction. Meanwhile, 37% Ag_3PO_4 was reduced for the pure Ag_3PO_4. This finding suggested that the HAp support improved the stability of Ag_3PO_4 and prevented its photoerosion (see Supporting information).

In general, the integration between the Ag_3PO_4 and HAp-773 accelerated the rate of photooxidation reaction under visible light irradiation, which can be attributed to the following reasons. Firstly, the microsphere morphology of HAp favors the transmission of the substrate. Secondly, the generation of the vacancy of HAp could act as a receiver, which not only make the efficient separation of the electron–hole pairs but also result in the production of the superoxide radicals. Besides, the support with calcination temperature at 773 K had enough OH species on the channel sites and PO_4^{3-} that was beneficial for the combination of the Ag^+ and the PO_4^{3-}, which could provide more photogenerated electrons to the HAp and generated more hole active sites on the Ag_3PO_4. Therefore, it is possible that the unique properties of the support created new charge-transfer paths and ultimately promoted the activity of the catalyst. Detailed theoretical calculation on this proposed mechanism is being underway.

4. Conclusions

In conclusion, the Ag_3PO_4/HAp composites were prepared by the in-situ ion exchange method and were applied in the photodecomposition of various pollutants. HAp, as a support, on the one hand, accelerated the transmission of dye molecule in the reaction; on the other hand, resulted in the formation of superoxide radicals with stronger oxidation ability. Therefore, the present study verified the presence of high efficiency of Z-scheme mechanism for the Ag_3PO_4/HAp composite, which demonstrated the creation of new charge-transfer paths and the promotion of charge transmission or separation, resulting in a significant enhancement in the photoactivity for pollutant removal under visible light irradiation. In addition, it was found that the calcination temperature had great influence on the ion exchange ability of HAp, thus, made the difference in the loading of Ag_3PO_4 on the support and the generation of the superoxide radicals in the system. The results and discussion herein provide valuable information for the further development of other Z-scheme mechanism type composite photocatalysts.

Acknowledgments

We would like to thank financial support by the Major State Basic Research Development Program (Grant No. 2012CB224804), NSFC (Project 21373054, 21173052), and the Natural Science

Foundation of Shanghai Science and Technology Committee (08DZ2270500).

Appendix A. Supplementary data

Supplementary data associated with this article can be found, in the online version, at http://dx.doi.org/10.1016/j.apcatb.2015.05.006.

References

[1] M.R. Hoffmann, S.T. Martin, W. Choi, D.W. Bahnemann, Chem. Rev. 95 (1995) 69–96.
[2] J.G. Yu, X.X. Yu, Environ. Sci. Technol. 42 (2008) 4902–4907.
[3] X.B. Chen, S.S. Mao, Chem. Rev. 107 (2007) 2891–2959.
[4] Z.G. Yi, J.H. Ye, N. Kikugawa, T. Kako, S.X. Ouyang, H. Stuart-Williams, H. Yang, J.Y. Cao, W.J. Luo, Z.S. Li, Y. Liu, R.L. Withers, Nat. Mater. 9 (2010) 559–564.
[5] Y.P. Bi, S.X. Ouyang, N. Umezawa, J.Y. Cao, J.H. Ye, J. Am. Chem. Soc. 133 (2011) 6490–6492.
[6] X.G. Ma, B. Lu, D. Li, R. Shi, C.S. Pan, Y.F. Zhu, J. Phys. Chem. C 115 (2011) 4680–4687.
[7] N. Umezawa, S.X. Ouyang, J.H. Ye, Phys. Rev. B 83 (2011) 035202.
[8] C.T. Dinh, T.D. Nguyen, F. Kleitz, T.O. Do, Chem. Commun. 47 (2011) 7797–7799.
[9] Y.P. Bi, S.X. Ouyang, J.Y. Cao, J.H. Ye, Phys. Chem. Chem. Phys. 13 (2011) 10071–10075.
[10] R. Asahi, T. Morikiwa, T. Ohwaki, K. Aoki, Y. Taga, Science 293 (2001) 269–271.
[11] J.J. Guo, S.X. Ouyang, P. Li, Y.J. Zhang, T. Kako, J.H. Ye, Appl. Catal. B: Environ. 134–135 (2013) 286–292.
[12] X.L. Fu, W.M. Tang, L. Ji, S.F. Chen, Chem. Eng. J. 180 (2012) 170–177.
[13] W.F. Yao, B. Zhang, C.P. Huang, C. Ma, X.L. Song, Q.J. Xu, J. Mater. Chem. 22 (2012) 4050–4055.
[14] Y.M. He, L.H. Zhang, B.T. Teng, M.H. Fan, Environ. Sci. Technol. 49 (2015) 649–656.
[15] L.L. Zhang, H.C. Zhang, H. Huang, Y. Liu, Z.H. Kang, New J. Chem. 36 (2012) 1541–1544.
[16] Z.H. Chen, F. Bing, Q. Liu, Z.G. Zhang, X.M. Fang, J. Mater. Chem. A 3 (2015) 4652–4658.
[17] X.F. Yang, H.Y. Cui, Y. Li, J.L. Qin, R.X. Zhang, H. Tang, ACS Catal. 3 (2013) 363–369.
[18] X.F. Yang, J.L. Qin, Y. Jiang, K.M. Chen, X.H. Yan, D. Zhang, R. Li, H. Tang, Appl. Catal. B: Environ. 166–167 (2015) 213–240.
[19] Y.P. Bi, S.X. Ouyang, J.Y. Cao, J.H. Ye, Phys. Chem. Chem. Phys. 13 (2011) 10071–10075.
[20] J.F. Ma, J. Zou, L.Y. Li, C. Yao, T.L. Zhang, D.L. Li, Appl. Catal. B: Environ. 134–135 (2013) 1–6.
[21] K.J. Zhu, K. Yanagisawa, A. Onda, K.J. Kajiyoshi, Solid State Chem. 177 (2004) 4379–4385.
[22] D. Aronov, A. Karlov, G. Rosenman, Eur. Ceram. Soc. 27 (2007) 4181–4186.
[23] D. Aronov, M. Chaikina, J. Haddad, A. Karlov, G. Mezinskis, L. Oster, I. Pavlovska, G. Rosenman, J. Mater. Sci.: Mater. Med. 18 (2007) 865–870.
[24] H. Kanai, Y. Matsumura, J.B. Moffat, Phosphorus Res. Bull. 6 (1996) 293–296.
[25] H. Nishikawa, K. Omamiuda, J. Mol. Catal. A: Chem. 179 (2002) 193–200.
[26] H. Nishikawa, J. Mol. Catal. A: Chem. 206 (2003) 331–338.
[27] H. Nishikawa, J. Mol. Catal. A: Chem. 207 (2004) 149–153.
[28] M.P. Reddy, A. Venugopal, M. Subrahmanyam, Appl. Catal. B: Environ. 69 (2007) 164–170.
[29] P. Rulis, L.Z. Ouyang, W.Y. Ching, Phys. Rev. B 70 (2004) 155104.
[30] T.S. de Araujo, S.O. de Souza, E.M.B. de Souza, J. Phys.: Conf. Ser. 249 (2010) 012012.
[31] H. Tounsi, S. Djemal, C. Petitto, G. Delahay, Appl. Catal. B: Environ. 107 (2011) 158–163.
[32] H. Sun, F.Z. Su, J. Ni, Y. Cao, H.Y. He, K.N. Fan, Angew. Chem. Int. Ed. 48 (2009) 4390–4393.
[33] A.M. Hu, T. Lei, M. Li, C.K. Chang, H.Q. Ling, D.L. Mao, Appl. Catal. B: Environ. 63 (2006) 41–44.
[34] K. Ozeki, J.M. Janurudin, H. Aoki, Y. Fukui, Appl. Surf. Sci. 253 (2007) 3397–3401.
[35] A.J. Nathanael, D. Mangalaraj, P.C. Chen, N. Ponpandian, Compos. Sci. Technol. 70 (2010) 419–426.
[36] J.J. Buckley, A.F. Lee, L. Olivi, K. Wilson, J. Mater. Chem. 20 (2010) 8056–8063.
[37] X.T. Hong, X.H. Wu, Q.Y. Zhang, M.F. Xiao, G.L. Yang, M.R. Qiu, G.C. Han, Appl. Surf. Sci. 258 (2012) 4801–4805.
[38] C.S. Pan, J. Xu, Y. Chen, Y.F. Zhu, Appl. Catal. B: Environ. 115–116 (2012) 314–319.
[39] M. Vukomanovic, V. Zunic, M. Otonicar, U. Repnik, B. Turk, S.D. Skapin, D. Suvorov, J. Mater. Chem. 22 (2012) 10571–10580.
[40] B.O. Fowler, Inorg. Chem. 13 (1974) 194–207.
[41] S. Klauer, M. Wöhlecke, S. Kapphan, Phys. Rev. B 45 (1992) 2786–2799.
[42] Q.J. He, Z.L. Huang, Y. Liu, W. Chen, T. Xu, Mater. Lett. 61 (2007) 141–143.
[43] G. Binder, G. Troll, Contrib. Mineral. Petrol. 101 (1989) 394–401.
[44] M. Ge, N. Zhu, Y.P. Zhao, J. Li, L. Liu, Ind. Eng. Res. Chem. 51 (2012) 5167–5173.
[45] J.D. Zhuang, W.X. Dai, Q.F. Tian, Z.H. Li, L.Y. Xie, J.X. Wang, P. Liu, X.C. Shi, D.H. Wang, Langmuir 26 (2010) 9686–9694.
[46] X.F. Hu, T. Mohamood, W.H. Ma, C.C. Chen, J.C. Zhao, J. Phys. Chem. B 110 (2006) 26012–26018.